Manipulating Stiffness of Biomechanical Systems to Train Muscle

by

Erik M. Thompson

Submitted to the Department of Mechanical Engineering in partial fulfillment of the requirements for the degree of

Bachelor of Science in Mechanical Engineering

at the

Massachusetts Institute of Technology

June 2022

© 2022 Erik M. Thompson All rights reserved.

The author hereby grants to MIT permission to reproduce and to distribute publicly paper and electronic copies of this thesis document in whole or in part.

Signature of Author:_____

Erik Thompson
Department of Mechanical Engineering
May 17, 2022

Certified by:_____

Ritu Raman
Assistant Professor of Mechanical Engineering
Thesis Supervisor

Accepted by:_____

Kenneth Kamrin
Associate Professor of Mechanical Engineering
Undergraduate Officer

Manipulating Stiffness of Biomechanical Systems to Train Muscle

by

Erik M. Thompson

Submitted to the Department of Mechanical Engineering on May 17, 2022
In partial fulfillment of the requirements for the Degree of
Bachelor of Science in Mechanical Engineering

ABSTRACT

A new design for the skeleton of biohybrid robots, millimeter scale soft robots powered by engineered muscle actuators, was developed to provide a binary change in stiffness. Two variations of the design were created, one using elastic 50A resin and the other PDMS. The elastic 50A resin design was fabricated successfully. The design uses a manually placed stiffening beam to create the desired change in stiffness. This would allow for the determination of the effects of training with higher stiffnesses after muscle differentiation. These biohybrid robots provide a test bed for studying engineered skeletal muscle and contribute to potential future applications in tissue engineering and biomechanical devices.

Thesis Supervisor: Ritu Raman

Title: Assistant Professor of Mechanical Engineering

Acknowledgements

I want to thank all my professors, teaching assistants, tutors, and friends who have helped me through the rigors of MIT and develop into a much better person because of it. In particular, I would like to thank Simona Socrate, both for teaching me Mechanics and Materials and helping me develop my ability to teach it to others via my experience as a teaching assistant in her class. This cemented my decision to continue mechanical engineering, as well as introduced me to Ritu Raman whom I would also like to thank. Words cannot express how thankful I am for the opportunity to learn from and contribute to her lab. I would also like to thank Martin Culpepper, who provided a significant amount of guidance over the course of writing this thesis, and from whom I hope I can continue learning from in the future. Finally, I would like to thank Tara Sheehan, Jenny Gao, Steven Wasserman, and Angel Bu for their help in my efforts, as it was indispensable in producing this thesis.

Contents

1 Introduction

Biological systems function based on the ability to sense and respond to signals on a variety of different scales[2]. Other qualities that are found in biological systems include replication, healing, and environmental adaptation[7]. These capabilities are almost non-existent in fully mechanical systems. When these characteristics are seen, the implementation is much less sophisticated than in their biological counterparts[4,7]. Therefore, the ability to produce and implement biological structures might allow the use of their unique qualities that are otherwise hard to replicate mechanically.

One of the first steps to implementing these structures is developing a way to provide an output using a biological structure. Many machines do this through the use of actuators, the biological equivalent of which is muscle[2]. Previous efforts have successfully applied engineered skeletal muscle to actuate biohybrid robots, soft robots powered by muscle, to produce an output[7]. In the case of this thesis, that output is locomotion.

Muscles show potential for applications as linear actuators, and in the case of biohybrid robots engineered skeletal muscles were able to produce forces up to 300μN [7]. While impressive, the force generated is much lower than that of primary skeletal muscle, which uses cells directly isolated from animal tissue and then grown in specialized medium[3]. To improve the force generation of engineered muscle, which is more sustainable and consistent in force production than primary muscle, exercise training during differentiation was applied and showed increases in force generation[7]. Following this result, it is reasonable to hypothesize that exercise training after differentiation could also improve force generation. This created the need for a biohybrid robot structure that can change stiffness to train the muscle post differentiation, the design of which is the purpose of this thesis.

While many solution paths exist, the current design focused on being producible in a simple and expedient manner. A PDMS skeleton was designed along with a PDMS “stiffener” which can be manually attached to provide the exercise training. The PDMS design would be cast in an 3D printed elastic 50A resin mold, which could be enlarged to produce as many skeletons as needed in one batch. An additional structure was designed to be 3D printed directly out of elastic 50A resin as well, which would likely be less quick to produce but also less labor

intensive. Both designs could help yield insights to the principles behind muscle growth, benefiting both this project as well as the field of tissue engineering.

2 Background

2.1 Biohybrid Robot Design

Previous biohybrid robots used a 3D printed skeleton, as well as a 3D printed ring mold to grow the muscle around the skeleton[8]. This skeleton was made out of PEGDA, which has a higher young's modulus than the PDMS or elastic 50A used in this thesis[6,7,11]. The biohybrid robots tend to use a structure of an upside down "U" shape with the muscle wrapped around the legs[7,8]. Locomotion is produced by a structural asymmetry, or an asymmetric triggering of one muscle band in the symmetric, multi- direction structure[7,8]. For this thesis, the two-leg structure will be the focus, of which one of the previous versions can be seen in Figure 2.1.

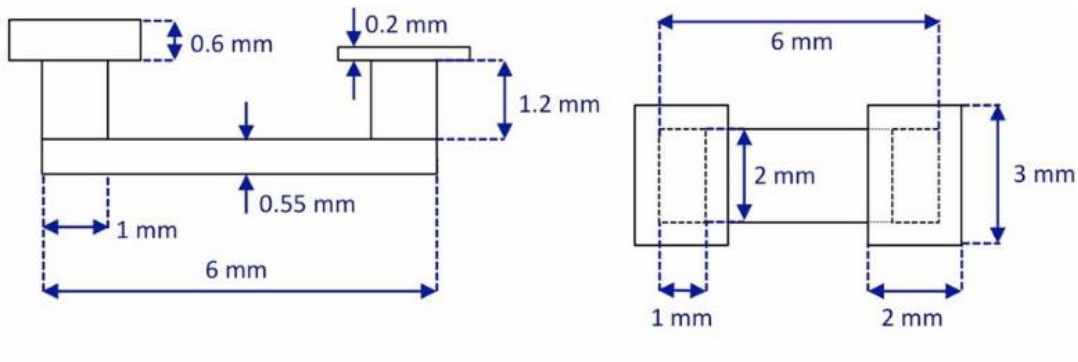

Figure 2.1: Bio bot with muscle attached[8]. The left depiction would be flipped upside down during use.

Utilizing this design has allowed for testing of various qualities of engineered muscle tissue, and it is the goal of this thesis to provide a design that can continue this testing. While not asymmetric, the new design will still allow for force to be determined from displacement as was done previously[7].

2.2 Engineered muscle tissue

The muscle used to power the biohybrid robots is engineered muscle tissue, which has a few important characteristics. First, the muscle cells have been transduced to respond to light in a

controlled manner[8]. This allows the muscle cells to be controlled non-invasively[8]. Additionally, they are grown in a ring shape which can be fitted over a variety of biomechanical machines[7,8]. The modified cells are C2C12 cells, a myoblast cell line that differentiates rapidly allowing for hastened production of the muscle rings[1]. The ability to produce muscle rings quickly and consistently is a substantial benefit over options such as primary cell lines that would introduce a large amount of variability in results depending on the original source[3,7]. The biohybrid robot design in this thesis is intended to use the same muscle rings as used previously.

3 Design

3.1 Design Requirements

The process of optimizing the biohybrid robot skeleton began by gathering design requirements. To produce a skeleton that would fit the desired role the requirements below were determined.

Table 3.1: Design Requirements

Low stiffness state	.5 N/m	± .29 N/m
High stiffness state	1.5 N/m	± .15 N/m
Deflection	.00079 m	± .00061 m

The design requirements were based on the need determined from lab testing of the muscles. The deflection given is the approximate range given by one of the existing skeletons and covers essentially the entire gap of the legs. Realistically, deflection will be dependent on the target stiffness states. Using the 300μN force as the maximum, this sets the target displacements to .6mm and .2mm for the low and high stiffness states respectively. Due to the lack of specific requirements for speed, weight, and some of the size dimensions, a variety of solutions could fill the current requirements. However, due to time constraints modifying the current beam structure of the biohybrid robot to satisfy the binary stiffness requirement became the optimal solution. The other promising design solution, which involves changing the stiffness using flexures, will be discussed further in the future work section.

3.2 Design Constraints

Due to using muscles as linear actuators, various unique design constraints also exist that must be considered. The various constraints are organized in the table below.

Table 3.2: Design Constraints

Muscle Length	Max 12mm inside perimeter of muscle loop
Environment	Submerged in fluid
Size	Must operate within a 35mm petri dish
Sterilization	Ethanol, UV, or high temperatures
Material	Biocompatible

One major design constraint is the biocompatible material for the skeleton of the biohybrid robot. In previous skeletons, a 33:1 ratio of PDMS was used to fulfill this requirement[9]. This material was again chosen to produce the skeletons in this thesis, despite having a few major drawbacks. The first drawback is that for the PDMS to work, it must be mixed with a curing agent and then cured in an oven. After curing, the PDMS is still extremely tacky and difficult to demold and use. Therefore, to speed the prototyping process skeletons were also designed and produced in Formlabs Elastic 50A Resin. It has a comparable Youngs modulus of .63 MPa, based on the stress at 50% strain from its technical data sheet[5]. The one issue with the elastic resin is it is not technically biocompatible. Some evidence exists that longer duration exposure to isopropyl alcohol after printing as well as longer exposure to UV light can remedy the cytotoxicity, but should be tested before using these skeletons[5]. As the skeletons would be a similar size to the previous biohybrid robots, the constraints related to the petri dish size would not be a concern, as well as constraints related to the process of attaching the muscle. Both PDMS and elastic 50A are also able to withstand sterilization temperatures, UV, and alcohol sterilization. The max muscle loop size was determined from previous skeleton sizes[8]. To reduce the chance of tearing the muscle during stiffness changes, max size of the muscle loop for the skeleton design would be approximately 12mm based on the distance and size of the legs.

3.3 Design Choices

As previously stated, two main design pathways stood out: flexures and a modified version of the current biohybrid robot skeleton. Using flexures would contribute towards the ability for a larger variety of applications in the long term. One flexure design could allow for ease of switching stiffnesses and be altered to other applications such as gripping. While a flexure design would be great for future applications, it would have been too much to achieve within the time frame of this thesis. Additionally, it still needs to be tested whether flipping stiffnesses would provide the changes in muscle to justify use of stiffness changing designs. Instead, a simple solution to provide a binary stiffness change that could be quickly produced using the same techniques as the current skeleton seemed more reasonable. The initial idea was based on adding a bar to either the upper or side beams, which would provide the required stiffness change. This opened up a variety of designs, including the one for this thesis of attaching a single bar below the upper beam. The final design that was chosen is shown in Figure 3.2.

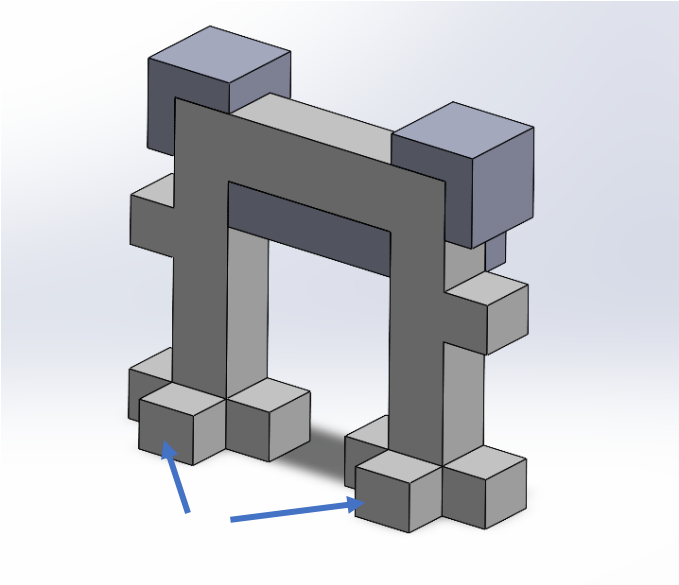

Figure 3.1: The two-part design of the skeleton and stiffener. To change stiffness the stiffener (dark grey) must be manually attached to or removed from the skeleton (light grey). The muscle would wrap around the two legs above the three toed feet. The blue arrow indicates the front toe of the foot.

A few other modifications were made based on information acquired outside of the design requirements. The two extra pieces on the legs were added to prevent the muscle from slipping over the top of the skeleton during placement. If this happens, the muscle might tighten up and become difficult to replace without tearing it. The front toe labelled in Figure 3.1 exists to support the stiffener which would otherwise cause the skeleton to fall. After selecting this design, calculations were applied to determine the optimal dimensions.

4 Formulas and Simulation

4.1 Mathematical analysis

Equations were derived from Euler–Bernoulli beam theory to give the displacement of the feet. A few assumptions were made to do this. First, the material was assumed to be isotropic, which for both PDMS and elastic 50A resin is acceptable[10,11]. Second, only small deformations were assumed, which is not completely accurate but is useful enough to inform the initial design. Third, the corners connecting the legs to the top bar were assumed to have negligible deformation. This is also not completely accurate, but for the same reason as before it was ignored. The last assumption made was treating the materials as linear elastic. While PDMS seems to be linear, elastic 50A resin is not[6]. However, since deformations in this situation will stay under 50% strain, linear elasticity was assumed. Due to symmetry of the structure, the displacement of one foot can be calculated by splitting the structure in half. The additional material on the leg added to help keep the muscle from slipping up the structure was also considered negligible. Finally, equation (4.4) can be derived using the assumptions above and the equations from beam theory applied in (4.1), (4.2), and (4.3).

$$\delta_{leg} = \frac{PL_1^3}{3EI_1} \tag{4.1}$$

$$\theta_{leg} = \frac{PL_1^2}{2EI_1} \tag{4.2}$$

$$\theta_{top} = \frac{M_P L_2}{EI_2} \tag{4.3}$$

$$\delta = \frac{PL_1^3}{3EI_1} + \frac{PL_1^2}{2EI_1}h_f + \frac{P\left(L_1+\frac{1}{2}h_2\right)L_2}{EI_2}\left(L_1 + \tfrac{1}{2}h_2 + h_f\right) \quad (4.4)$$

The first term of (4.4) is from (4.1) and provides displacement due to simple bending of the leg beam. Because the load is applied above the foot, the second term was added to provide the displacement at the bottom of the foot. It comes from multiplying (4.2) by the height of the foot h_f. The last term accounts for the displacement of the bottom of the foot due to deformation of half of the top beam from moment M_p. It was provided by multiplying the angle at the end of the top beam from (4.3) with the total distance to the bottom of the foot from the centerline of the top beam. I_1 and I_2 are the bending moments of inertia for beam one, the leg, and beam two, the top beam. Superposition allows us to combine these terms to find the overall displacement δ in (4.4) due to a load P. Deformations due to axial compression of the top beam were ignored. Figure 4.1 is provided to clarify the variables.

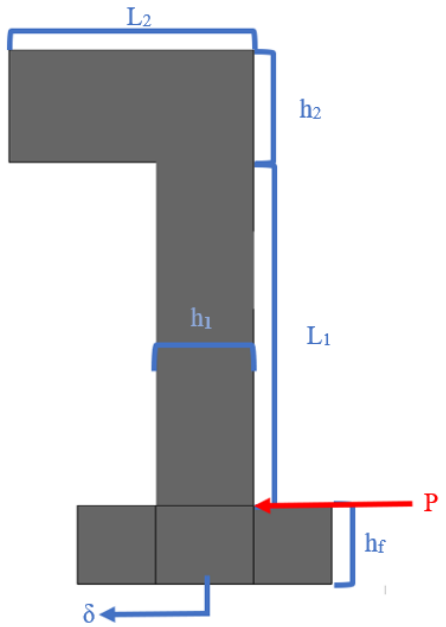

Figure 4.1: The upper left face of the beam is considered fixed. Moment of Inertia is calculated based on the width into the board *b*.

In much the same way, the equation for the deformation of the stiffened structure can be calculated. Another assumption is required; the top beam and the stiffening beam are fully attached. In reality, there is nothing binding the beams together but since both materials have

large amounts of friction when interacting and the geometry of the structure forces the stiffening beam into the top beam during loading, this assumption was accurate enough to suffice. Equation (4.5) allows for the calculation of the stiffened displacement.

$$\delta_{stiff} = \frac{P(L_1-h_3)^3}{3EI_1} + \frac{P(L_1-h_3)^2}{2EI_1}h_f + \frac{P(L_1+\frac{1}{2}(h_2-h_3))L_2}{EI_{2+3}}(L_1 + \frac{1}{2}(h_2-h_3)+h_f) \quad (4.5)$$

Equation (4.5) is similar to the previous (4.4) with a few minor differences. All terms come from the same components as before, but now account for the functional length change for the leg beam due to bar 3. Figure 4.2 illustrates the variables in the new setup.

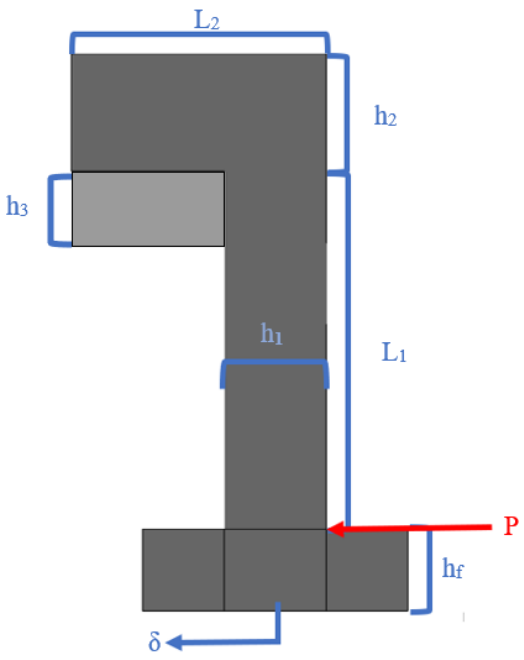

Figure 4.2

The last quantity of importance is the overall stiffness of the structure. This was simply calculated by dividing the load applied by the deformation. The only change made to the equations were removing the h_f variable as well as terms used to account for the foot in order to get displacement in the same horizontal plane as the load.

4.2 FEA and Analysis

To get the final geometric dimensions, the previous equations were used to find initial values to unknown dimensions for a skeleton made of PDMS and for one made of elastic 50A. To reduce the complexity of molding, the width of the part, variable *b*, was set to 1mm. This allowed for the skeleton to be molded sideways with no components reaching extraordinary depth into the mold. Doing this made it necessary to keep the leg height $h_{1,}$ as well as the space between the legs, sum up to 5mm as any longer would risk tearing the muscle rings. To satisfy this requirement, the height of the legs h_1 was set to 1mm. Future skeleton designs should modify these values to provide optimal dynamic behavior, but for the purpose of this thesis that was not needed. This left L_1, h_2, and h_3 as the values that could be manipulated to fulfil the requirements.

L_1 and h_2 were determined first, as h_3 is not part of the underlying skeleton and requires a known stiffness of the skeleton itself. Figure 4.3 and Figure 4.4 show predicted deformation while varying leg length and top beam height.

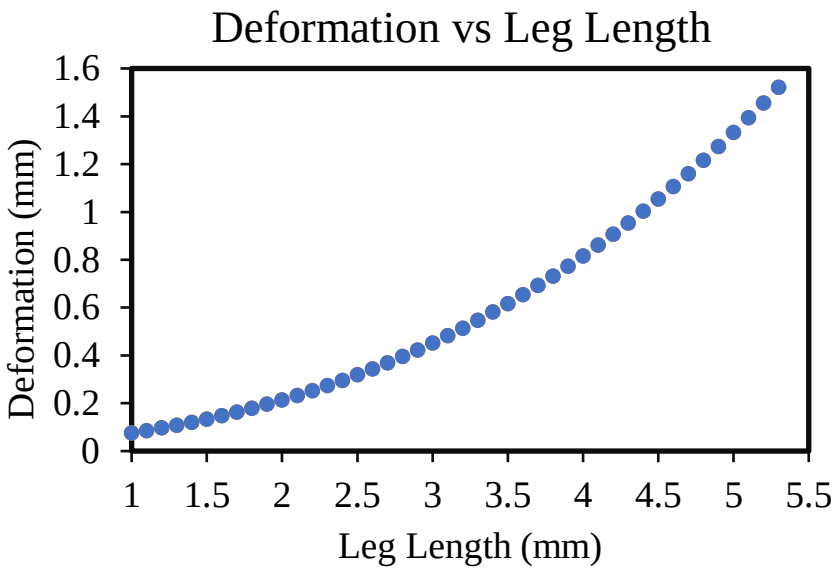

Figure 4.3: Predicted deformation over varying leg lengths. The height of the top beam h_2 was held constant at 1mm.

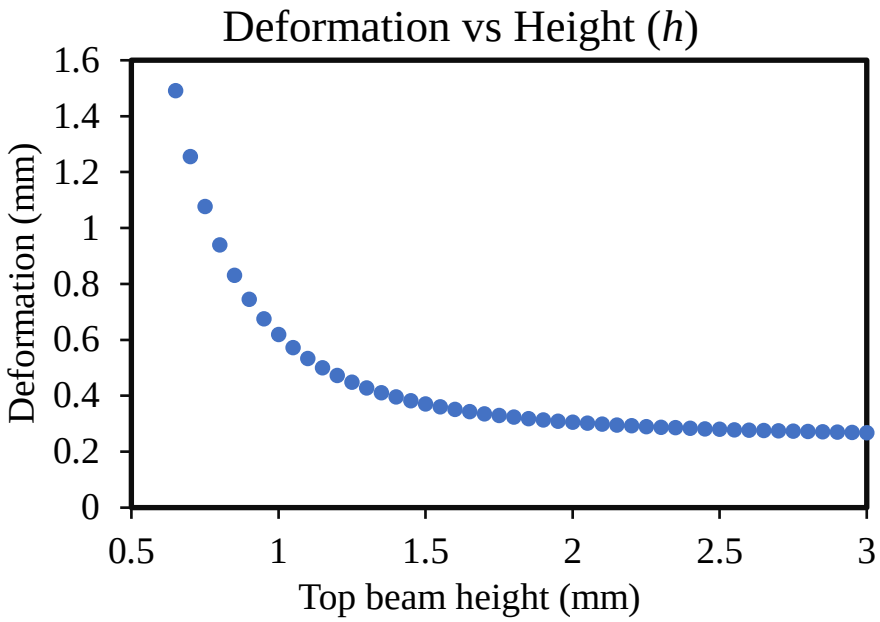

Figure 4.4: Predicted deformation over varying top beam heights. The leg length L_1 was held at a constant 3.5mm.

As can be seen in the first graph, a height of around 3.5mm produced a deformation of around .55mm. As this was already taller than the original skeleton, L_1 was held at 3.5mm as then h_2 could be manipulated to be around 1mm to adjust to .6mm deflection. The predicted value of h_2 to provide this deformation was 1.08 mm. Considering the assumptions previously made, the calculation was expected to overestimate stiffness and the optimal value should be larger. FEA was conducted in anticipation of displacement being larger than desired. The results of the unstiffened FEA are shown in Figure 4.5.

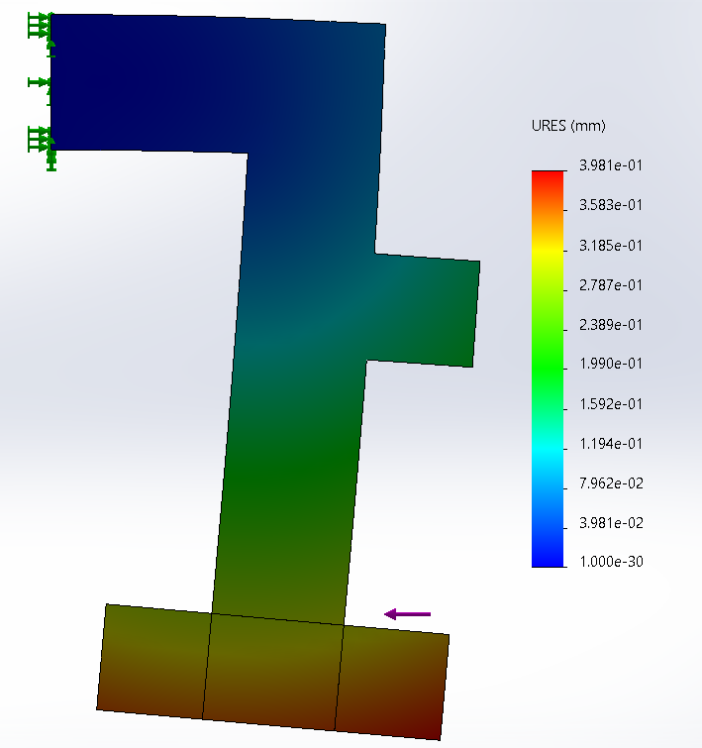

Figure 4.5: FEA of half of the structure under a point load of .0003N. Displacement of the center of the foot was .37mm with an h_2 of 1.08mm.

As can be seen, the simulated displacement was larger than the target .3mm. As said before this was likely due to the assumptions made, but the models were still accurate enough to be used with a slight adjustment. To do this, the simulated displacement value was divided by the desired value to produce a coefficient to multiply in the original equation for deflection. Solving for h_2 with the coefficient then produced the new value of 1.15mm. Figure 4.6 shows the secondary FEA simulation used to confirm this value.

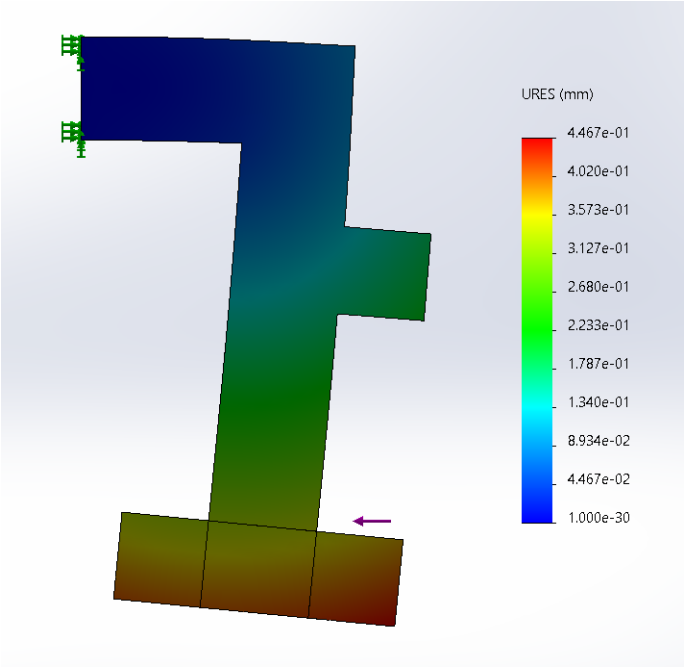

Figure 4.6: FEA with a h_2 of 1.15mm. Deflection at the base of the foot was 31mm.

The simulation showed that with an h_2 of 1.15mm, the total deflection would be around .62mm which was acceptable. For future testing it also seemed beneficial to have a range of variation since the muscle is not attached in the exact same way every time. To provide a tentative lower bound to deformation as well as ensure the structure would function under a more realistic scenario, the FEA simulation in Figure 4.7 was applied with a load distributed between the foot and slide stop. This is because the muscle might stretch further up the leg and act less like an optimal point load. For testing with muscle, the area on the leg the muscle acts over should be used to calculate the force generated. For designing to achieve the stiffness required, a point load is reasonable as the design is intended for the maximum displacement possible.

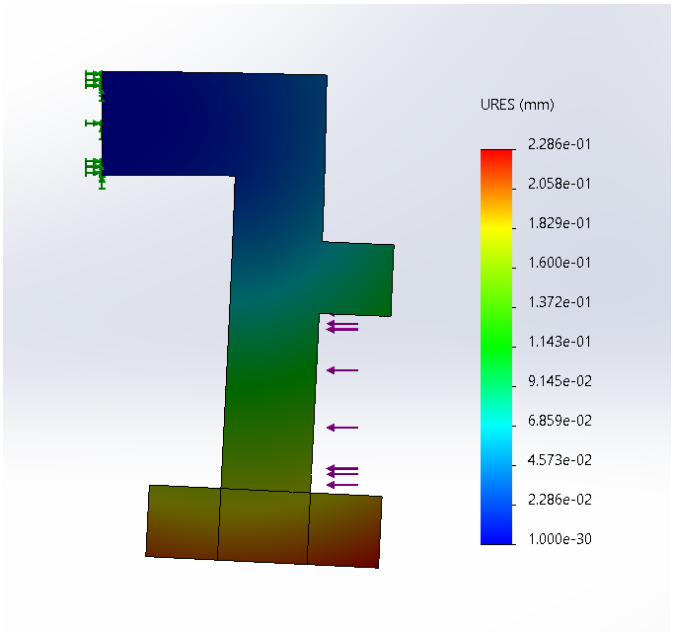

Figure 4.7: Distributed load FEA. The deformation was 21mm, about 23% lower than in Figure 4.6.

The last step was to determine h_3. In the exact same process, h_3 was first calculated to be .60mm. FEA simulation predicted a displacement of .12mm. Then, using a new coefficient h_3 was calculated to be .811mm and verified in a final FEA to produce the desired deflection. Figure 4.8 and Figure 4.9 display the FEA simulations.

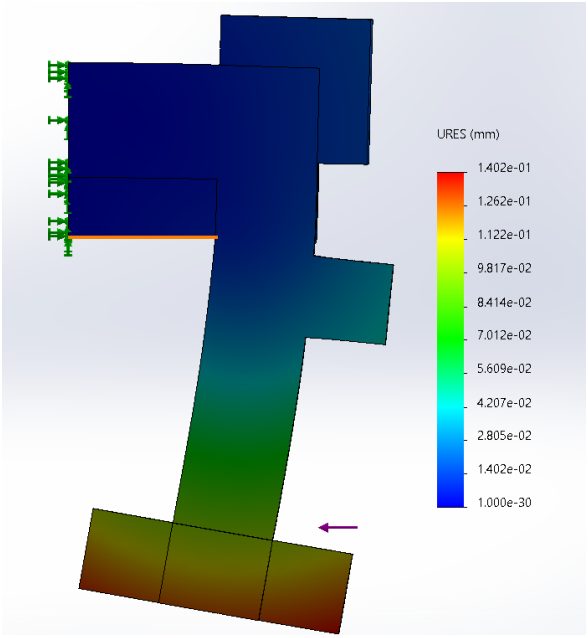

Figure 4.8: FEA with h_3 = .60mm and deflection of .12mm

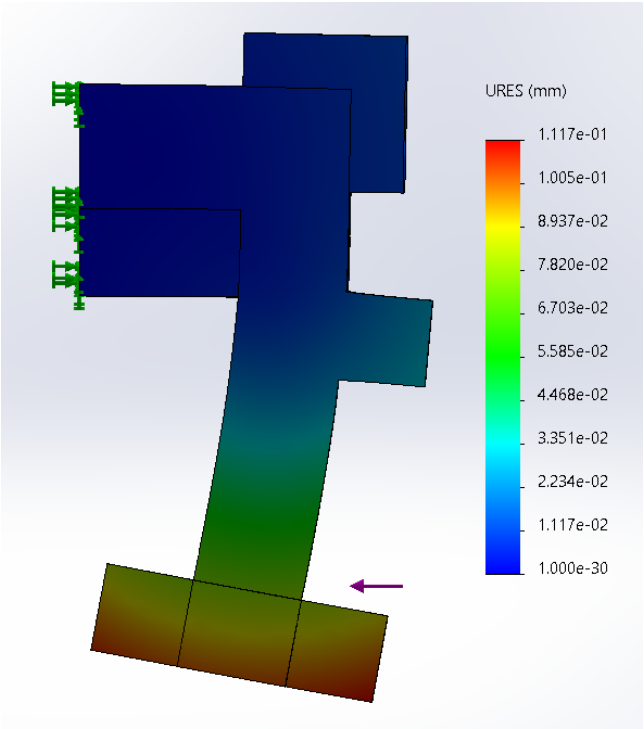

Figure 4.9: FEA with h_3 = .81mm and deflection of .10mm

The same analysis was conducted for a skeleton made from the elastic 50A resin. The leg length was still held at 3.5mm, and the initial h_2 calculation was .95mm. After FEA, h_2 was calculated and verified at 1.08mm. Repeating the process again for the stiffened structure resulted in an initial h_3 of .62mm and a final h_3 of .73. Figure 4.10, Figure 4.11, Figure 4.12, and Figure 4.13 show the FEA at these various stages.

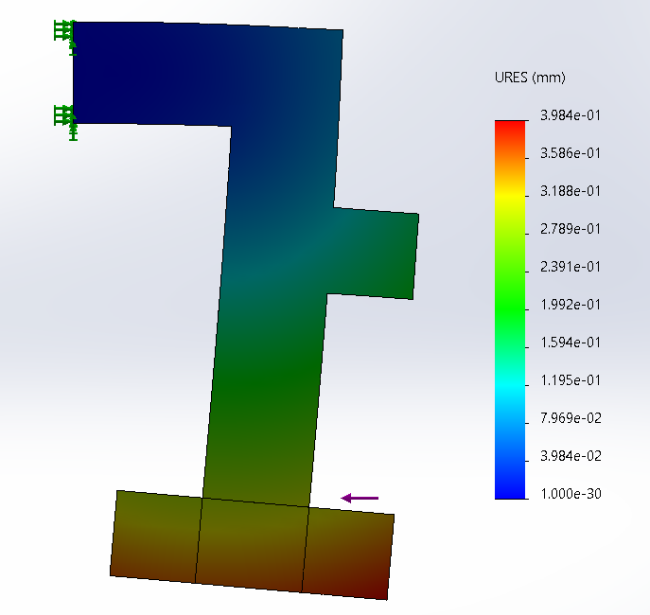

Figure 4.10: FEA with h_2 = 95mm and deflection of .37mm

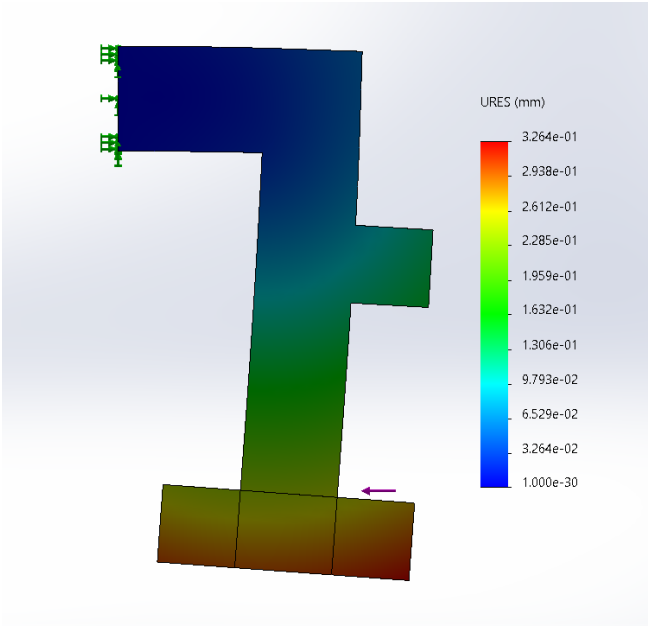

Figure 4.11: FEA with h_3 = .108mm and deflection of .30mm

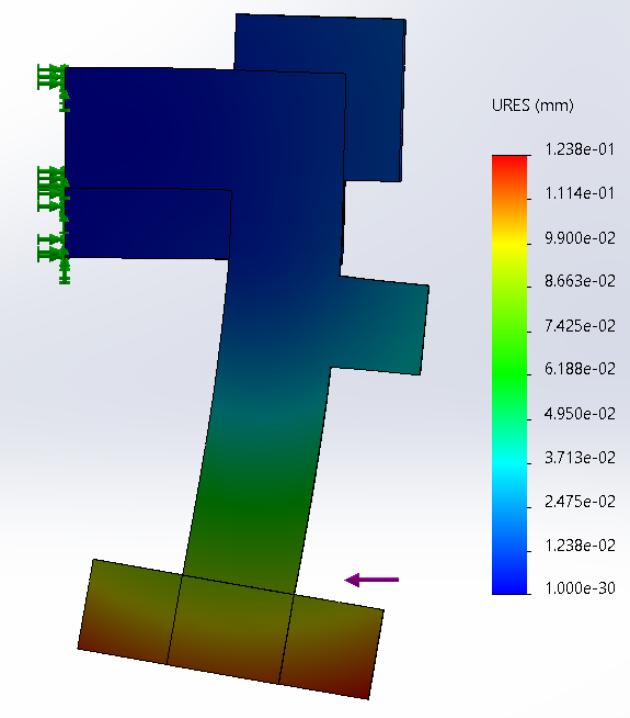

Figure 4.12: FEA with h_3 = .62mm and deflection of .114mm

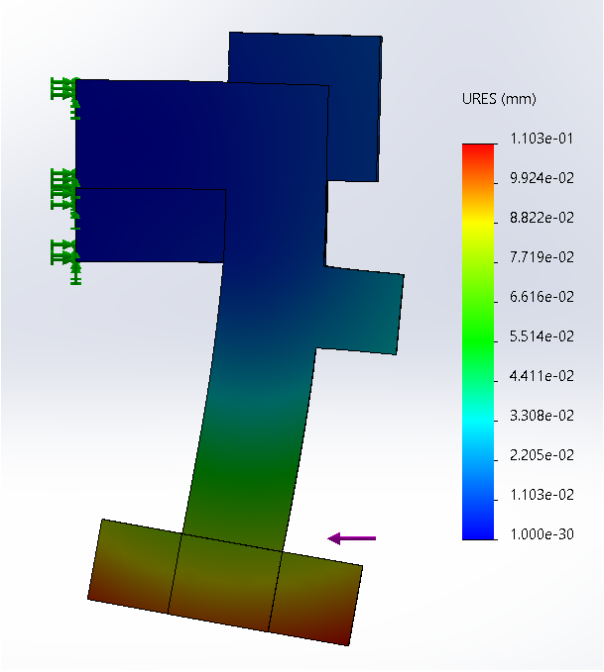

Figure 4.13: FEA with h_3 = .73mm and deflection of .10mm

5 Fabrication

5.1 Elastic 50A

After determining the necessary dimensions, fabrication of the elastic 50A skeletons and stiffeners was relatively straight forward. They were printed in a Formlabs Form 3 printer, rinsed for 20 minutes in isopropyl alcohol, dried for 20 minutes, and finally cured for 20 minutes. Due to the size of the part, printing directly on the build platform would likely have caused it to be too difficult to remove the parts without breaking them. Therefore, a support structure was required. The supports have an approximate diameter of one millimeter at the interface with the part, which after removal still left sizeable lumps on the part in a few areas. While unlikely to ruin experiments conducted with these skeletons, the extra material might provide added stiffness.

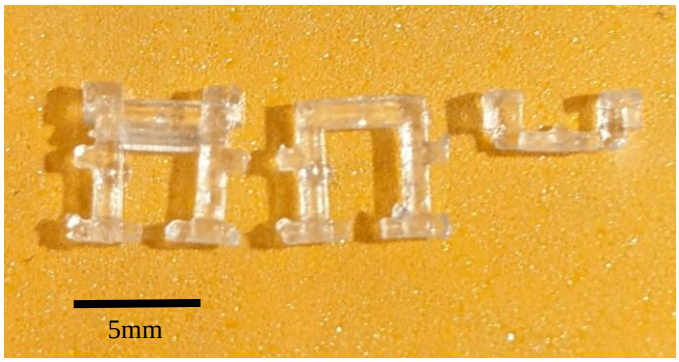

Figure 5.1: From left to right: Skeleton with stiffener, skeleton without stiffener, stiffener alone.

5.2 PDMS

Efforts to produce the PDMS parts were unsuccessful, but mostly due to difficulties using the material and not the mold itself. The first step in producing these parts was creating the mold. The initial molds were made with Formlabs white resin, but due to the size of the parts and the resolution of the printer the molds came out unusable. The final mold was created after altering the design of the parts to be better suited to casting. The mold was also printed in elastic 50A resin, as the pliability of the mold was intended to aid with demolding the PDMS parts.

Figure 5.2: Mold for PDMS skeletons.

However, testing of the mold showed the ratio of elastomer base to curing agent was likely off as the parts never became solid enough to remove from the mold. While the mold used did not work, it is unlikely that either its material or its flexibility caused its failure. More efforts should be made to determine better molding practices to increase the ease of use for PDMS.

6 Conclusions

6.1 Conclusions

In this thesis, a new biohybrid robot skeleton was designed and simulated to provide a test bed to determine how changes in resistance experienced by the muscles affect their ability to generate force when used as a linear actuator. It is currently understood that both optical and mechanical stimulation of the muscle rings during differentiation provides an increase in muscle performance[8]. Providing mechanical stimulation after differentiation could potentially yield similar benefits, and the biohybrid robot skeleton designed in this thesis provides a platform to both test and iterate on. The advances in our understanding of engineered muscle functioning produced from experimenting with biohybrid robot contributes to potential future applications in medicine, industry, and a variety of other spaces where actuators are used currently.

6.2 Future work

A significant amount of work remains both for the new biohybrid robot design as well as further in this area of research. While the new skeleton and stiffener have been rigorously simulated with FEA, there are factors such as variation in production, material consistency, and variation in muscles that necessitate testing of the current design. Both testing with the muscle rings, as well as testing with the skeleton alone, would provide useful insights as to the limits in producing these structures and where improvements to the design can be made.

Further efforts toward the flexure-based design also warrant attention. Especially on this small of a scale, traditional methods for creating joints become much harder to implement when compared to flexures. Additionally, flexures open the door to controlling changing stiffness between two states via bistable structures. If implemented, this could eventually make it easier to remotely change the stiffness of a biohybrid robot.

Developing the ability to use muscles for application outside of the lab is one of the larger areas to direct future work efforts. Creating a way to protect and feed the muscles outside of a petri dish, improving the method of attaching the muscles to the structures they actuate, and increasing size of muscles grown would all heighten the ability to apply engineered muscle actuators outside of the current biohybrid robots. Additionally, furthering understanding of muscle dynamics and enhancing the ability to get sensor feedback at a small scale will be crucial to creating a usable control system to actuate the muscles with the accuracy needed to apply them for most situations.

7 Bibliography

[1] *C2c12*. ATCC. (n.d.). Retrieved May 15, 2022, from https://www.atcc.org/products/crl-1772

[2] Chan, V., Asada, H. H., & Bashir, R. (2013, November 28). *Utilization and control of bioactuators across multiple length scales*. Lab on a Chip. Retrieved May 14, 2022, from https://pubs.rsc.org/en/content/articlelanding/2014/LC/C3LC50989C

[3] Dennis, R. G., Kosnik, P. E., Gilbert, M. E., & Faulkner, J. A. (2001, February 1). *Excitability and contractility of skeletal muscle engineered from primary cultures and cell lines*. American Journal of Physiology-Cell Physiology. Retrieved May 14, 2022, from https://journals.physiology.org/doi/full/10.1152/ajpcell.2001.280.2.C288

[4] Feinberg, A. W. (n.d.). *Biological Soft Robotics*. Annual Reviews. Retrieved May 15, 2022, from https://www.annualreviews.org/doi/10.1146/annurev-bioeng-071114-040632

[5] Grigaleviciute, G., Baltriukiene, D., Bukelskiene, V., & Malinauskas, M. (2020, March 10). *Biocompatibility Evaluation and enhancement of elastomeric coatings made using table-top optical 3D printer*. MDPI. Retrieved May 15, 2022, from https://www.mdpi.com/2079-6412/10/3/254

[6] *Material Data Sheet Elastic 50A*. (2019, January 7). Retrieved May 14, 2022, from https://formlabs-media.formlabs.com/datasheets/2001420-TDS-ENUS-0.pdf

[7] Raman, R., Cvetkovic, C., & Bashir, R. (2017, February 9). *A modular approach to the design, fabrication, and characterization of muscle-powered biological machines*. Nature News. Retrieved May 14, 2022, from https://www.nature.com/articles/nprot.2016.185#Sec1

[8] Raman, R., Cvetkovic, C., Uzel, S. G. M., & Bashir, R. (2016, March 14). *Optogenetic skeletal muscle-powered adaptive biological machines*. Retrieved May 14, 2022, from https://www.pnas.org/doi/10.1073/pnas.2114639119

[9] Raman, R., Cvetkovic, C., & Bashir, R. (2021). *Muscle-Powered Biological Machines* (U.S. Patent No. 10,906,169). U.S. Patent and Trademark Office. https://patentimages.storage.googleapis.com/a6/d0/44/c9e5102c4b2386/US10906169.pdf

[10] *Validating isotropy in SLA 3D printing*. Formlabs. (n.d.). Retrieved May 14, 2022, from https://formlabs.com/blog/isotropy-in-SLA-3D-printing/

[11] Wang, Z., Volinsky, A. A., & Gallant, N. D. (2014, May 22). *Crosslinking effect on polydimethylsiloxane elastic modulus measured by ...* Retrieved May 14, 2022, from http://volinsky.myweb.usf.edu/PDMSCompression.pdf